ARTICLE

pubs.acs.org/est

Quantitative High-Resolution Mapping of Phenanthrene Sorption to Black Carbon Particles

Martin Obst,[†] Peter Grathwohl,[†] Andreas Kappler,[†] Oliver Eibl,[‡] Nicola Peranio,[‡] and Tilman Gocht[†,*]

[†]Center for Applied Geoscience, Eberhard Karls University Tuebingen, Hölderlinstr. 12, 72074 Tuebingen, Germany

[‡]Institute for Applied Physics, Eberhard Karls University Tuebingen, Auf der Morgenstelle 10, 72076 Tuebingen, Germany

Supporting Information

ABSTRACT: Sorption of hydrophobic organic contaminants such as polycyclic aromatic hydrocarbons (PAHs) to black carbon (BC) particles has been the focus of numerous studies. Conclusions on sorption mechanisms of PAH on BC were mostly derived from studies of sorption isotherms and sorption kinetics, which are based on batch experiments. However, mechanistic modeling approaches consider processes at the subparticle scale, some including transport within the pore-space or different spatial pore-domains. Direct evidence based on analytical techniques operating at the submicrometer scale for the location of sorption sites and the adsorbed species is lacking. In this work, we identified, quantified, and mapped the sorption of PAHs on different BC particles (activated carbon, charcoal and diesel soot) on a 25−100 nm scale using scanning transmission X-ray microscopy (STXM). In addition, we visualized the pore structure of the particles by transmission electron microscopy (TEM) on the 1−10 nm-scale. The combination of the chemical information from STXM with the physical information from TEM revealed that phenanthrene accumulates in the interconnected pore-system along primary "cracks" in the particles, confirming an adsorption mechanism.

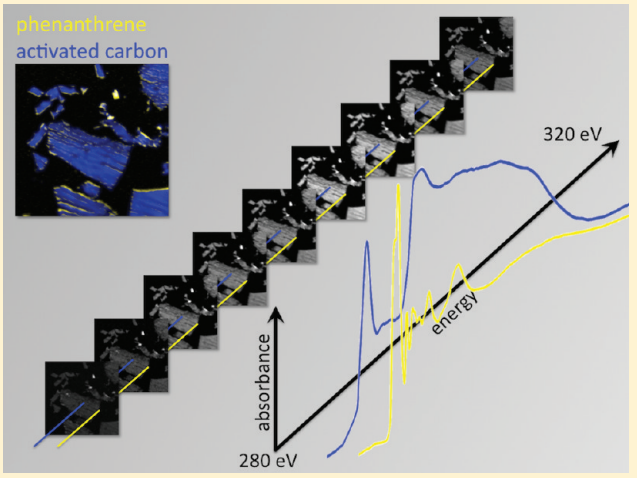

INTRODUCTION

Black carbon (BC) particles play an important role for the fate of hydrophobic organic pollutants (HOCs). In soils and sediments these particles have been identified as important sorbents for the pollutants.[1,2] Because of strong sorption, the presence of BC particles reduces aqueous concentrations and mobility of pollutants [3,4] and therefore their bioavailability.[5] This has been carried forward to the design of on-site environmental engineering concepts that aim to reduce bioavailability of organic pollutants at contaminated sites.

Numerous studies were conducted to investigate the mode of sorption (*ab*sorption versus *ad*sorption) of HOCs on organic matter in soils and sediments. On the basis of nonlinear sorption isotherms it has been proposed that adsorption is the dominant mechanism of HOCs on BC particles.[1,6] Consequently, sorption parameters were correlated with surface properties (such as the specific surface area and the pore size distribution[7]) in order to validate models for the assessment of equilibrium sorption coefficients. However, the underlying mechanisms involved in the sorption processes were so far mainly addressed with indirect methods and interpretations about interactions between solutes and sorbents were predominantly derived from macroscopic observations.[6,8,9] Hence, complementary studies using analytical techniques that operate at the subparticle scale potentially provide direct evidence for the involved sorption mechanisms.

To this end, two-step laser desorption/laser ionization mass spectrometry (L^2MS) has been applied to localize HOCs such as polycyclic aromatic hydrocarbons (PAHs) on selected sorbents including BC particles.[10−13] However, a major drawback of L^2MS is that the analytes need to be transferred into the gas phase prior to ionization and subsequent analysis using time-of-flight mass spectrometry. Consequently, the direct observation of adsorbed compounds is not possible with that technique.

As an alternative, synchrotron-based soft X-ray spectroscopy has been established recently in the environmental sciences for quantifying the distribution of chemical species at the subparticle scale. In particular, scanning transmission X-ray microscopy (STXM) that combines speciation capabilities of near-edge X-ray absorption fine structure spectroscopy (NEXAFS) with ∼25 nm spatial resolution were used as a powerful method for characterizing the carbon pool in soils and sediments on the subparticle level. NEXAFS revealed chemical heterogeneities between surface near and interior areas of BC particles.[14−16] Moreover, it has been shown that STXM is even capable of

Received: April 5, 2011
Accepted: July 15, 2011
Revised: July 5, 2011
Published: July 15, 2011

mapping HOCs such as polychlorinated biphenyls on BC particles.[17]

On the basis of currently available knowledge, we assume that HOC sorption on BC particles is dominated by adsorption and, therefore, the HOC distribution should follow the physical structure of the particles (porous network). The overall goal of this work is to validate this assumption by a combination of analytical microscopy techniques. We used STXM in our study for mapping phenanthrene as a model compound for HOCs on different organic sorbents, namely charcoal (CC), diesel soot (DS), and activated carbon (AC). The objectives were (i) to detect phenanthrene on structures that are chemically similar (i.e., aromatic rings on sorbents with high aromaticity) and (ii) to locate the sorption domains at the subparticle level within the porous structure that was elucidated by means of transmission electron microscopy (TEM).

EXPERIMENTAL SECTION

Phenanthrene Sorption Experiments. Three different types of BC were analyzed regarding their sorption capacity and spatial distribution of phenanthrene sorbed to the particles: (i) activated carbon (F100, Chemviron Inc., Calgon Carbon Corp., Pittsburgh, USA), (ii) charcoal (Sommerhit, Chemviron Inc., Calgon Carbon Corp., Pittsburgh, USA), and (iii) diesel soot (reference material SRM 2975, obtained from the National Institute of Standards and Technology (NIST); Gaithersburg, ME, U.S.). These materials were studied previously with respect to sorption of organic compounds [18,19] and, based on that, the batch experiments could be designed so as to achieve high phenanthrene loadings as the ideal condition for the chemical mapping using STXM. Pulverized samples of activated carbon and charcoal with a grain size <63 μm (sieved) were used in the sorption experiments. The primary soot particles size is 34 $\pm$ 9 nm, but these particles form aggregates. However, 90 vol% of the aggregates are <70 μm in diameters.[20] Further detailed characterizations of the BC particles can be found elsewhere.[18,19]

The batch sorption experiments are described in detail in the Supporting Information (see Experimental Section, Supporting Information). Briefly, the BC particles were suspended in deionized water, spiked with phenanthrene solutions (5 g L^{-1} dissolved in MeOH) and NaN_3 was added to inhibit bacterial growth. After an equilibration time of 3 weeks the sorbed amount of phenanthrene was quantified via the liquid phase concentrations by means of gas chromatography (Hewlett-Packard 5890)/mass spectrometry (Hewlett-Packard 5972). The sedimented solids were separated from the aqueous phase by carefully removing the supernatant using pipettes and dried under a stream of nitrogen. Losses of phenanthrene to the air are limited through the high log K_{OA} ($\sim$7.5;[21]) and additional loadings from the water phase were kept at a minimum as only 1−2 mL of water were evaporated.

Sample Preparation. For spectromicroscopic identification and quantification of the phenanthrene sorption to BC, the particles need to be ultrathin sectioned, which requires embedding of the particles. The conventional approach, i.e. the embedding in epoxy resin, would obscure and modify the spectral signature of the sorbent and the sorbate at the C1s absorption edge. Therefore, the particles were embedded in liquid elemental sulfur for sectioning, followed by the sublimation of the sulfur. Aliquots of a few μg of elemental sulfur were heated up on a microscopy glass slide until they just melted ($\sim$110−115 °C). Small liquid sulfur droplets with a diameter of approximately 0.5 mm were then mixed with the BC particles and the droplet was cooled down to room temperature within 2−3 min. The droplets were glued onto glass bars and ultramicrotomed to a thickness of approximately 100 nm using Reichert OM U3 and Leica EM UC7 Ultramicrotomes with diamond knifes (Diatome, Switzerland). The sections were deposited on Formvar coated 200 mesh Cu grids. At room temperature, the sulfur, which was used as embedding medium, sublimated within two days. A potential influence of the embedding procedure on the distribution of the sorbed phenanthrene is evaluated in the discussion section.

Scanning Transmission X-ray Microscopy and Data Analysis. The sections were analyzed by scanning transmission X-ray microscopy (STXM) at the beamline 10ID-1 at the Canadian Light Source (CLS) within a week subsequent to the sample preparation. All STXM measurements were done under 1 atm of He. The microscope energy scale was calibrated regularly to an accuracy of $\pm$0.05 eV using the Rydberg peaks of gaseous CO_2. For sample analysis, STXM was used in image sequence mode.[22] Image sequences were recorded across the C-1s absorption edge (280−320 eV, 147 energy steps in total) with an energy resolution of 0.1 eV in the spectral region of interest and broader energy steps in the pre-edge region (<284 eV) and above the absorption edge (>293 eV). The raw, transmitted signals were converted to linear absorbance scale (optical density, OD) according to eq 1 using the software package aXis2000:[23]

$$\mathrm{OD} = -\ln(I \cdot I_0^{-1}) \quad (1)$$

where I [s^{-1}] is the transmitted flux through the sample and I_0 [s^{-1}] is the incident flux measured in an empty region adjacent to the analyzed particles. Quantitative chemical species maps were derived from the OD image sequences by linear decomposition using the singular value decomposition algorithm of aXis2000.[23] Thereby, the NEXAFS spectrum of each individual pixel is fitted by a linear combination of spectra of pure reference compounds normalized to an efficient thickness of 1 nm.

Reference Spectra. Reference spectra were recorded previously from pure sorbent materials, which were prepared as the other samples. Spectra were extracted from image stacks across the C1s edge of the bulk area of three or more adjacent particles of each of the sorbent materials. The spectra were extracted in an iterative process by mapping both the respective sorbent material and aromatic contamination (using the phenanthrene spectrum as a model compound; note that the initial, "native" concentrations of phenanthrene on the sorbents—measured via chemical extraction—is <0.1% of the amount after the sorption experiment for each of the sorbents, see Table S2, Supporting Information). Mapping was followed by masking the pure sorbent areas wherefrom the spectra were finally taken. The used reference spectra are average spectra of more than 5200, 5900, and 3900 individual spectra (pixels of the image stack) for AC, CC, and soot, respectively.

The phenanthrene reference sample was prepared by wet deposition of $\sim$2 μL droplets of a solution of 5 g L^{-1} phenanthrene (Aldrich 695114−5G, Sigma Aldrich Chemie GmbH, Munich, Germany) dissolved in MeOH followed by the evaporation of MeOH at room temperature. NEXAFS spectra were derived from stacks of regions wherein the maximum optical density was <1.5 OD units to avoid problems with absorption saturation which would distort the reference spectra.[24] The reference spectrum of phenanthrene used for mapping is the

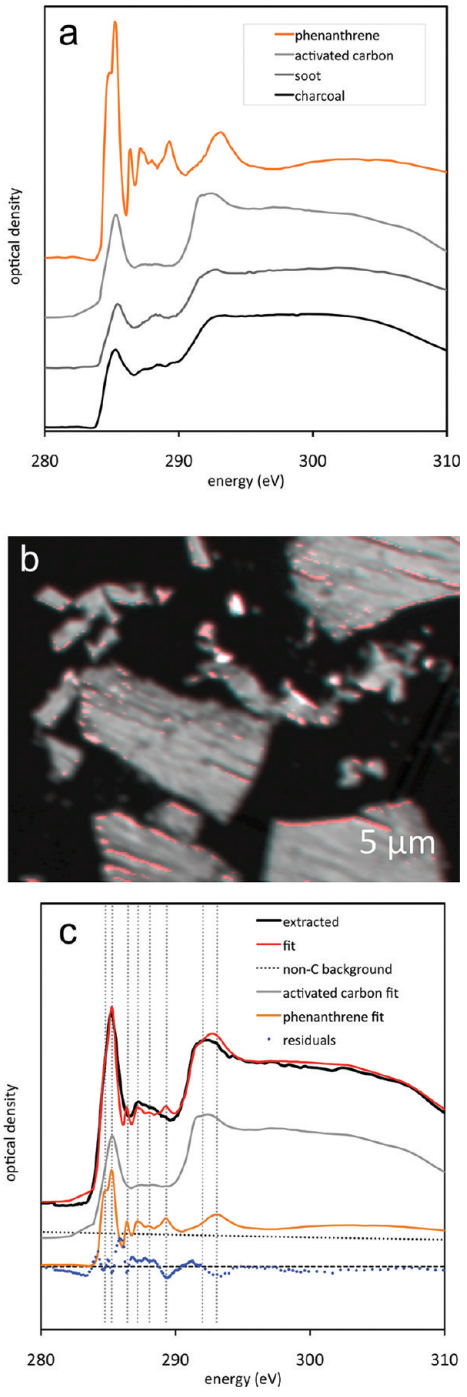

Figure 1. (a) C1s NEXAFS spectra of phenanthrene (orange), activated carbon (light gray), soot (gray) and charcoal (black) recorded by STXM. (b) STXM image (average across C1s edge, OD) of ultrathin sections of activated carbon. Areas of high phenanthrene contents are marked red. (c) Example of spectral fitting of STXM NEXAFS spectra. The red spectrum was derived from the area marked in b. This spectrum was fitted (gray) as a linear combination of the previously determined reference spectra of pure phenanthrene (orange) and AC (light gray).

average of 830 individual spectra (pixels in an image stack). For quantitative visualization, the resulting spectra were divided by a factor to normalize the edge-jump to a theoretical value that was calculated for an effective thickness of 1 nm using the atomic scattering factors.[25]

Transmission Electron Microscopy (TEM). In addition to the spectromicroscopical STXM experiment we also analyzed the samples by TEM to visualize the pore structures of the different sorbents at high spatial resolution. TEM experiments were carried out on a Zeiss 912 Ω TEM equipped with an Omega energy filter and operated at an acceleration voltage of 120 kV. Energy-filtered bright-field images were acquired using a 5−10 eV energy slit and an objective aperture with acceptance angle of 3 mrad. Fresnel contrast in bright-field images using out of focus conditions allows to image pore-structures on the nm-scale [26−28] and was applied here.

Image Processing for Visualization. The species maps obtained from STXM and the TEM images were slightly distorted with respect to each other. This could either have been caused by nonlinearities of the scanning motion in the STXM scans, or by slight deformation of the Formvar-membranes in the electron beam in the TEM. The latter is more likely since the deformation was not restricted to the line scanning direction of the STXM. For visualization, overlays of the STXM-derived phenanthrene maps onto the TEM-images the distortions were corrected manually. All quantifications were done without any spatial correction on the species-maps obtained from STXM (uncorrected original maps are presented in Figures S3, S4 and S5, Supporting Information).

RESULTS AND DISCUSSION

Quantitative Phenanthrene Mapping on Individual Carbon Particles. Although phenanthrene and the three types of BC particles are similar in terms of their chemical composition and rich in aromatic rings, and can therefore be similar with regard to their C1s NEXAFS spectra,[29] we were able to map the adsorption of phenanthrene to single BC particles. The main prerequisite for this approach is the possibility of distinguishing between the compounds using their C1s NEXAFS fingerprints.

The spectra of the 3 sorbents were similar to each other and all three were significantly different from the phenanthrene spectrum (Figure 1a). The three sorbents showed absorption peaks characteristic for the C1s→π^* transition of aromatic or graphite-like C=C bonds at 285.3 eV (AC, CC) or 285.4 eV (DS). Beyond the aromatic absorption peak all three spectra show only a few features up to 290 eV such as minor, broad peaks at 287.3 and 288.3 eV, followed by broad peaks characteristic for C1s→σ^* transition of sp2 hybridized C-atoms at 291.7 and 292.5 eV (AC) or 291.7 and 293 eV (DS and CC).

In contrast, the phenanthrene spectrum showed a number of distinct absorption peaks at 284.8, 285.2, 286.4, 287.2, 288.0, 289.3, and 293.0 eV. The first two transitions are the excitations of the lowest unoccupied molecular π^* orbital (LUMO) and the next higher energy state (LUMO+1; compare Agren et al.[30]). The absorption peaks at higher energies are caused by excitations of unoccupied σ-orbitals of the conjugated aromatic molecule.

The observed differences in the absorption spectra between phenanthrene and the three carbon-based sorbents suggested the possibility of quantitatively fitting the absorption spectrum of a mixture by using a linear combination of the reference spectra of the individual compounds. Phenanthrene-rich regions were selected for this purpose (Figure 1b). The principle of the linear combination fitting is illustrated in Figure 1c. The resulting fit is similar but not equal to the measured spectrum (the standard deviation of the fit is 0.022 OD units). The differences are very likely due to the interaction of the planar phenanthrene molecule

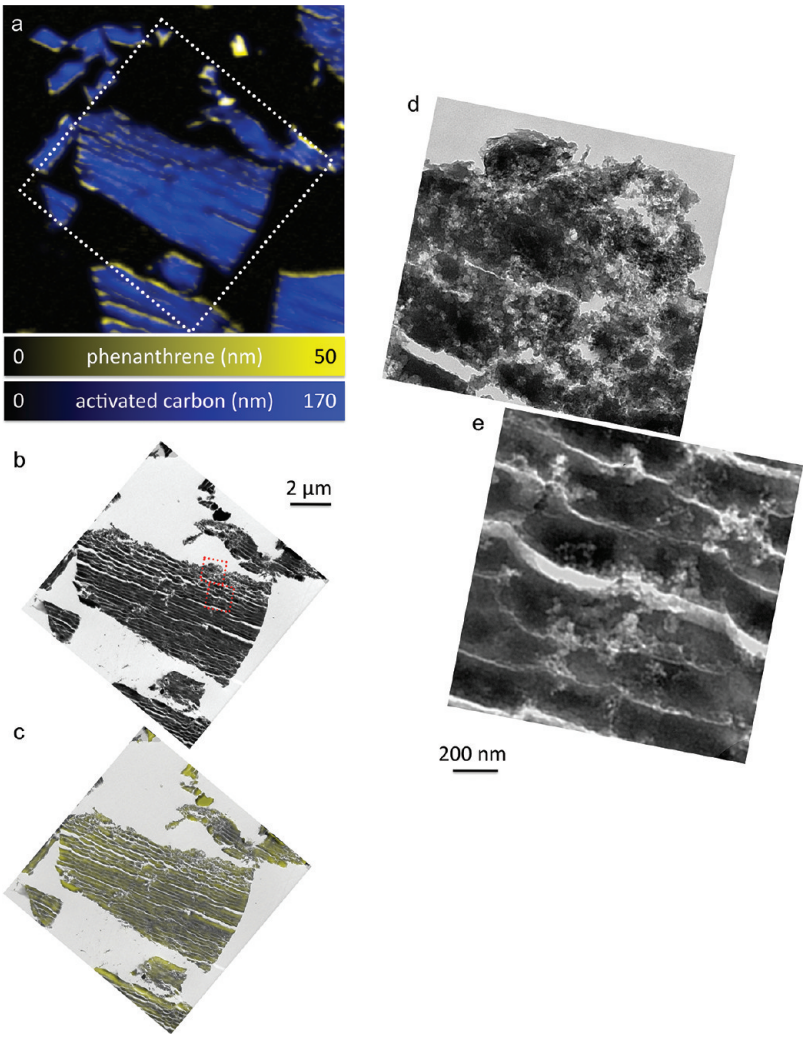

Figure 2. (a) Color overlay of quantitative species maps of phenanthrene (yellow) sorbed to activated carbon (AC, blue) as obtained from STXM image sequences across the C1s edge. Color scales represent the effective thickness of the individual compounds in nm. (b) TEM micrograph of the same AC particle visualizing the high porosity of the material. (c) Overlay of phenanthrene map obtained by STXM and the corresponding TEM bright-field image b. Regions are marked red in b at which bright-field TEM images were recorded at higher magnification (d, e).

with the sorbent surfaces. Detailed explanations can be found in the Supporting Information.

Distribution of Phenanthrene Sorbed on Activated Carbon. Figure 2a shows a color overlay of quantitative species maps of both phenanthrene (yellow) and AC (blue). The majority of phenanthrene was accumulated at the external surface of the particles as well as the surfaces of cracks visible throughout the ultrathin section of the activated carbon particles. The spatial resolution of STXM (~25 nm) allows for visualization of the macropores (>50 nm). However, we also observed phenanthrene in the "bulk" structure of the activated carbon particles, which we assumed to be sorbed inside the meso- (2−50 nm) and micropore (<2 nm) structure that can only be partly resolved by STXM (pore size definitions according to IUPAC [31]).

To visualize the meso- and micropores, we analyzed the samples by TEM. Figure 2b shows a bright-field image of the same section of the particle that was previously studied by STXM. The mesopore-structure of the AC particle was well resolved by the electron microscope (see also enlarged regions in Figures 2d, 2e). The micropore-structure was more difficult to visualize since the pore diameter was found to be only a few nm. We were able to partly visualize the micropore-structure using Fresnel contrast in TEM bright-field images and thereby applying slight overfocus (see Figures S7−S10 and S12, Supporting Information). Under these conditions, nanosized pores appear in dark contrast. The overfocused images revealed that micropores not only occur in close approximation to the meso- and macropores, but also within the bulk material.

The color overlay of the STXM phenanthrene distribution map and the TEM image (Figure 2c) suggests that macro- and mesoporous domains as for example shown on top of the large particle are not necessarily associated with the highest phenanthrene accumulations. In contrast, phenanthrene accumulates predominantly at the edges of the large pores and within the adjacent regions. Considering the more or less homogeneous distribution of micropores as revealed by TEM bright-field image focus series (see Figure S7, Supporting Information) we conclude that large parts of the micro- and mesoporous domains were not occupied by phenanthrene after three weeks of equilibration in the batch sorption experiment. This could possibly be due to unconnected pores located at a distance of

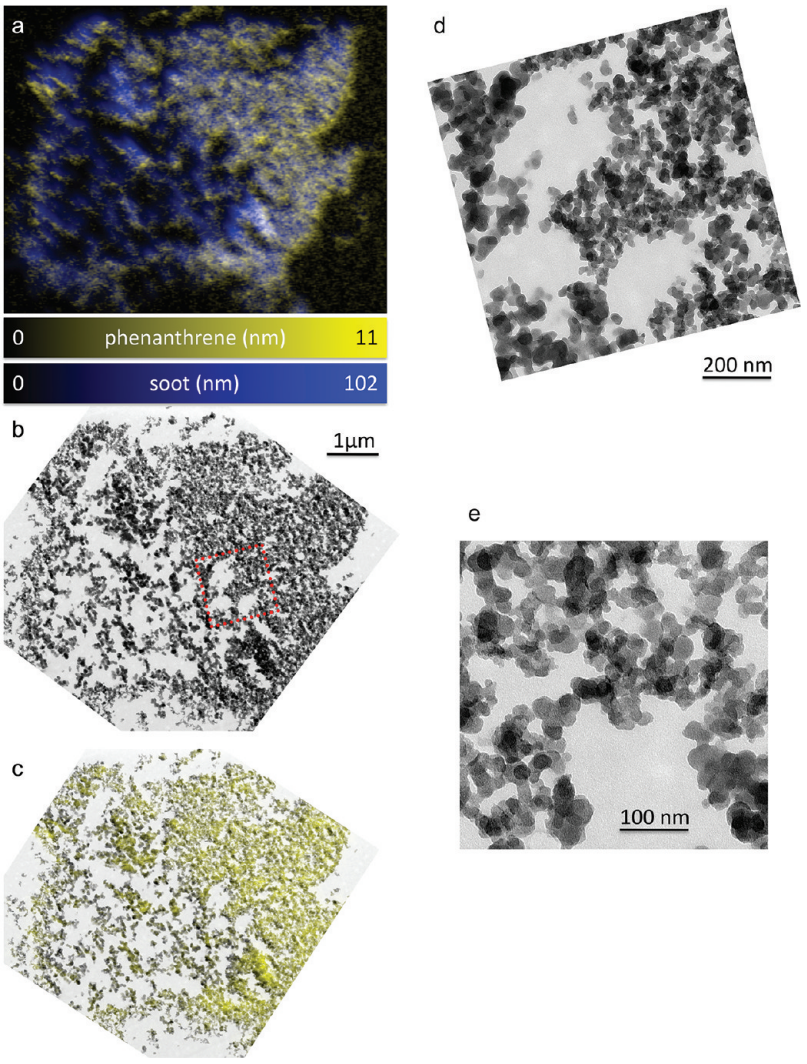

Figure 3. (a) Color overlay of quantitative species maps of phenanthrene (yellow) sorbed to diesel soot (DS, blue) as obtained from STXM image sequences across the C1s edge. Color scales represent the effective thickness of the individual compounds in nm. (b) TEM micrograph of the same soot aggregate imaging the high porosity of the aggregate that consists of primary particles of 10−50 nm in size. (c) Overlay of phenanthrene map obtained by STXM and the corresponding TEM bright-field image b. (d) Bright-field TEM image at higher magnification of the region marked red in b. (e) Bright-field TEM images at higher magnification, showing the agglomeration of primary soot particles.

the macropores, or extremely slow diffusion kinetics in the microporous domain.

The total amount of phenanthrene sorbed to the analyzed AC particles as determined by STXM was approximately 10.8% wt. of the AC particle, calculated with an assumed density of 1 g cm^{-3} for AC and 1.2 g cm^{-3} for phenanthrene. A comparison with untreated AC showed approximately 4.4 wt % of aromatic compounds, most likely caused by C−H bonds present at the surface of BC particles or PAH, which matched the phenanthrene C1s spectrum more closely as compared to the AC spectrum and therefore shows up in the phenanthrene maps. The native phenanthrene concentration on AC as revealed by solvent extraction and subsequent analysis is negligible (less than 0.01 ‰ compared with the spiked samples, see Table S2, Supporting Information). The background content of aromatic compounds spectroscopically similar to phenanthrene seemed to be significant, but its role in interacting with phenanthrene is unclear. Most likely, these are high molecular weight compounds with high aromaticity and containing C−H bonds, maybe part of the AC structure and not extractable by organic solvents. Note that the sorbent reference spectra were taken in an iterative approach from particle areas low in "phenanthrene" (see Experimental Section, Reference Spectra).

The STXM-derived loading of AC with phenanthrene was about 1/4 of the value of bulk chemical measurements in the aqueous phase of 22.2% wt (obtained from the mass-balance in sorption experiments, see Table S2, Supporting Information), which matches reasonably well considering the fundamentally different approaches and fits with the expected loading at this equilibrium aqueous concentration reported in literature for the same type of AC.[19] The difference between bulk and single particle based measurements could be caused by various reasons such as potential desorption of phenanthrene from the ultrathin sections during sectioning or transport (see below).

Distribution of Phenanthrene Sorbed on Diesel Soot. Unlike AC and CC, diesel soot used in this study is not a compact structure but formed from aggregates of primary particles of 34 ± 9 nm in diameter. Thus, the pore structure is not a primary,

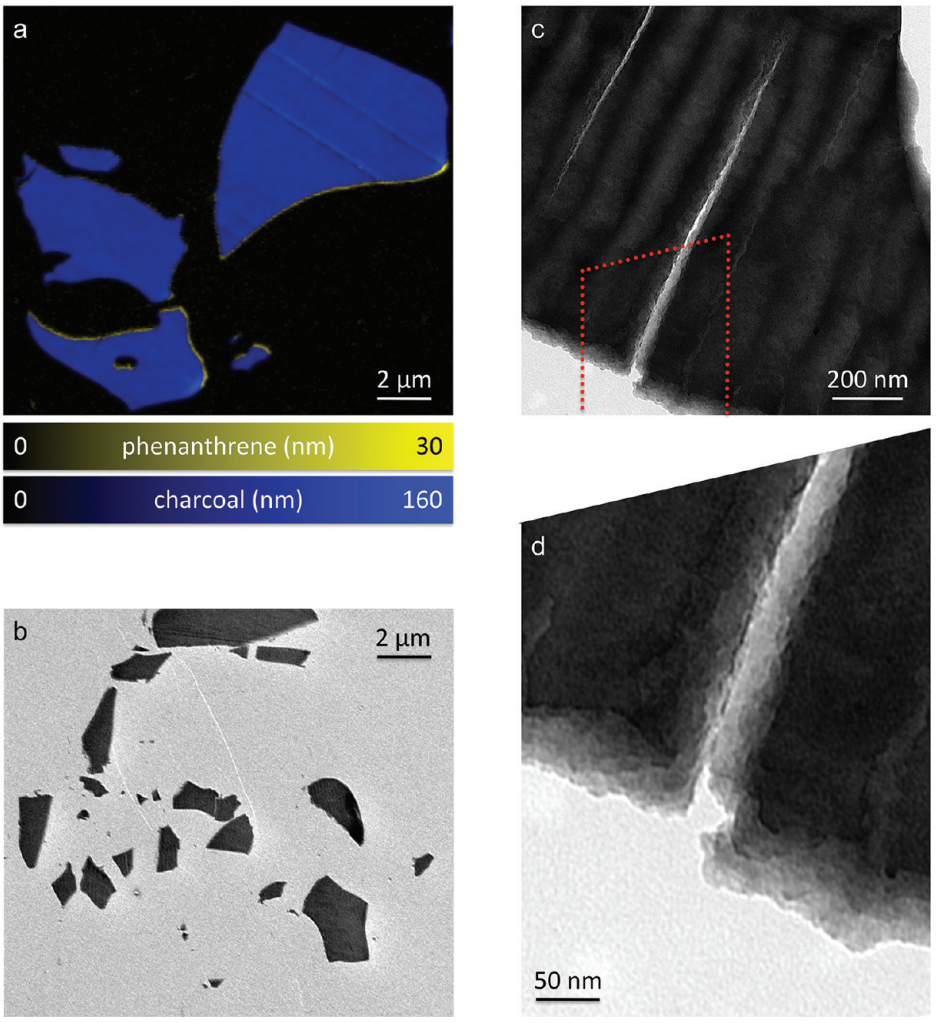

Figure 4. (a) Color overlay of quantitative species maps of phenanthrene (yellow) sorbed to charcoal (CC, blue) as obtained from STXM image sequences across the C1s edge. Color scales represent the effective thickness of the individual compounds in nm. (b) TEM micrograph of CC particles at the same magnification as in a, visualizing the rather low porosity of the material. (c). Bright-field TEM image of one of the cracks through the CC particle. (d) Bright-field TEM image at higher magnification of the region marked red in c.

stable pore structure but the result of secondary aggregation. Figure 3a shows a color overlay of quantitative distribution maps of phenanthrene and the soot. The distribution of phenanthrene appears much more homogeneous throughout the DS aggregate. To better resolve the structure of the aggregate, the same ultrathin section was studied by TEM as well. A bright-field TEM image is shown in Figure 3b. The pores within the aggregate appear more uniformly distributed and perfectly isotropic in contrast to AC (Figure 2) and CC (Figure 4). The porosity appeared to be higher as compared to AC and much higher as compared to CC. Figure 3c shows an overlay of the STXM phenanthrene map and the low-magnification TEM bright-field image.

Figure 3d shows the structure of the same DS aggregate at higher magnification. TEM bright-field imaging (red box in Figure 3b) revealed a particle size of about 30 nm. The high porosity and the connectivity of the pores within the aggregate are clearly observed. At higher magnification, the onion-like internal structure of the primary particles, and of the aggregation of the DS particles is depicted in the TEM bright-field image shown in Figure 3e. This structure could be verified by recording an electron diffraction pattern of a soot aggregate (see Figure S13, Supporting Information).

The amount of phenanthrene sorbed by DS as obtained from STXM image sequence measurements was lower as compared to AC. We observed a 3.2 wt % difference between phenanthrene treated and untreated material. This result was almost perfectly in agreement with our results from our bulk measurements with 4.2 wt % adsorption of phenanthrene (see Table S2, Supporting Information). In general, high sorption capacity and affinity of DS aggregates can be expected considering the high porosity, pore connectivity and homogeneous distribution of phenanthrene within the DS aggregate as suggested by Figure 3b.

Distribution of Phenanthrene Sorbed on Charcoal. Figure 4a shows a color overlay of phenanthrene (yellow) sorbed to CC (blue). Phenanthrene was accumulated mainly at the external surfaces and within the few intraparticle pores. The maximum local concentrations are similar to those observed for AC and soot, but the distribution is by far less homogeneous since less internal surface area is available for the sorption of phenanthrene. The CC particles were much more compact and the porosity was much smaller as compared to the activated

carbon and the aggregates of soot as observed by TEM. Unfortunately, we were not able to analyze the same particle since the Formvar film in this area was not stable in the electron beam and broke prior to the analysis. Thus, transmission electron micrographs of adjacent, smaller particles are shown in Figure 4b, which were obtained from the same ultrathin section, but from a different square of the TEM grid. Higher magnification images were acquired (Figure 4c) and verified the absence of any significant meso- and microporosity using the same Fresnel-contrast approach as for the AC (see Figure S10, Supporting Information). Figure 4d shows the crack of Figure 4c at higher magnification. Even at the interfaces of the crack, the material appears to be rather compact.

The low porosity as obtained from electron microscopy might explain the lower sorption capacity of CC as compared to AC and DS. On the basis of STXM image sequence measurements, we observed a difference of 1.7% wt. between phenanthrene treated and untreated material. This concentration is higher as estimated from the differences in aqueous concentrations, which was 0.6% wt.

Comparison of Sorbents. Out of all three sorbent materials, AC had the highest sorption capacity for phenanthrene as determined both by aqueous phase measurements as well as by quantitative spectromicroscopy measurements of single particles, followed by DS and finally by CC. The single particle based observations (STXM) are in principle in agreement with batch experimental data, although deviations in both directions of up to a factor of 3 (AC, CC) or smaller (DS) were observed. The phenanthrene distribution follows the physical structure at the subparticle scale, suggesting surface coating or pore-filling as dominant sorption mechanism. Consequently, adsorption rather than absorption controls the sorption process in sorbents with high intraparticle porosity, which is in line with the state-of-the-art theory regarding sorption of HOCs (reviewed, e.g., by Allen-King et al.[6]) that were developed based on data from bulk measurements. However, as parts of the microporous network were not occupied by the sorbate, there is no obvious relationship between the pore-size distribution and the phenanthrene distribution. It should be noted that high phenanthrene loadings close to the saturation level were used in this pilot study and the distribution among the porous network may be different at lower concentrations.

Critical Evaluation of the Spectromicroscopy Approach. For the first time, we could visualize and to some extent quantify the sorption at the scale of macro- and meso-pores. Some of the limitations of this approach, however, cannot directly be measured and quantified, but they need to be considered and discussed in detail.

Potential Artifacts from Sample Preparation. We decided to use a carbon-free embedding in liquid sulfur in this work to preserve the organochemical composition of the samples to the best possible extent. Liquid sulfur embedding does not obscure the NEXAFS C1s spectroscopic signature of the sorbent and sorbate and allows for sectioning and sublimating the embedding sulfur at room temperature and under ambient pressure. The main disadvantage of this method is the relatively high temperature of 110−115 °C to which the whole particles are exposed for up to two minutes during the embedding, but prior to sectioning. We cannot fully exclude all potential possibilities for a redistribution of phenanthrene during the embedding procedure. However, on the basis of our observations, we assume that this is limited because of the following considerations: A potential redistribution might happen through desorption and dissolution of phenanthrene in liquid sulfur. However, we did not observe phenanthrene signatures subsequent to sectioning and deposition on the Formvar-coated grids in areas adjacent to the particles, which prior to sublimation were covered by the sulfur. This indicates that no major amounts of phenanthrene were associated with the liquid sulfur phase. Furthermore, assuming a pore-filling mechanism for sorption of phenanthrene one would in particular expect desorption from the macropores. Our results clearly show that phenanthrene is still present in the macropores indicating that desorption to the sulfur phase is fairly limited. In summary, despite the temperature of 110−115 °C, the short period of 2 min is not expected to result in major changes of the phenanthrene distribution, although we cannot rule it out completely.

Losses may occur during sublimation of the sulfur at room temperature over 2 days, but taking into account the high log K_{OA} (~7.5 [21]) and the strong sorption properties of BC particles this should be limited. Furthermore, we could detect phenanthrene on external particle surfaces of all studied sorbents that should be affected by losses through evaporation. However, as the particles were highly loaded, evaporation of phenanthrene during removal of the sulfur may be a relevant loss mechanism.

Evaluation of the Linear Combination Fitting Approach. The accuracy and precision of the linear combination fitting approach used for the identification of sorbed phenanthrene has been previously evaluated and discussed.[32] In brief, the approach is mostly limited by systematic errors, not by statistic errors and the quality of the fits depends on the choice of the appropriate reference compounds. These limitations are essentially due to differences between the NEXAFS spectra of pure and adsorbed phenanthrene. As shown in Figure 1c, the spectrum extracted from PAH-rich areas of the section is not an exact match of the sum of the spectra of BC and phenanthrene. The differences are presented quantitatively as an exemplary spectrum in Figure 1c and as the spatially resolved residual signals in the Figures S3−S5 (Supporting Information) for AC, CC, and soot respectively. Significant differences between the NEXAFS spectra of the pure and the adsorbed compound due to strong sorption of planar PAH molecules to sorbent surfaces have been described in the literature [33,34]. Hence, we attribute these differences to the sorption process of phenanthrene.

However, we did observe a significant increase of the mapped phenanthrene content in the samples that were previously equilibrated with phenanthrene as compared to the raw material. Since no other compounds were added in our experiments, this is a clear indication that the measured differences are caused by the sorbed phenanthrene. More information can be found in the Supporting Information.

Implications for Studying Environmental Processes. In this pilot work, STXM enabled a proof-of-concept with respect to sorption theory. High phenanthrene loadings on the sorbents were anticipated, as this provides the highest probability to detect the sorbate on chemically similar surfaces. The results clearly show that mapping of phenanthrene on BC particles at the submicrometer scale is indeed feasible. However, environmental concentrations of phenanthrene are typically much lower as compared to this work. As chemical mapping relies on spectral differences between treated and untreated material, the applicability for analyzing phenanthrene sorption to field samples may be limited due to a high potential for sorption of unknown, nontarget compounds, which makes the interpretation of the

spectral information very difficult, if not impossible. In contrast, STXM applications in the context of HOC sorption are very promising for studying processes in well-defined model systems at the bench scale. For instance, the phenanthrene distribution among the pore space may be different at lower concentrations, which could be investigated using the combination of STXM with TEM. Furthermore, it was proposed that coating of BC particles with organic macromolecules may lead to a reduced sorption capacity due to a molecular sieving effect.[35] STXM offers the opportunity to study such effects based on direct observations and, thus, may further improve the understanding of diffusion processes at the subparticle scale.

■ ASSOCIATED CONTENT

Supporting Information. Schematic of the sample preparation workflow (Figure S1), statistical information of the reference spectra used for quantitative mapping (Table S1 and Figure S2), detailed descriptions of the batch sorption experiments (including Table S2), original species maps derived from STXM (Figures S3−S5), detailed interpretation and critical evaluation of the spectral fitting and mapping approach, structural information derived from TEM (Figures S6−S12) and a TEM electron diffraction pattern from a soot aggregate (Figure S13) are presented in the Supporting Information. This material is available free of charge via the Internet at http://pubs.acs.org.

■ AUTHOR INFORMATION

Corresponding Author

*Phone: +49-(0)7071-29 73149; Fax +49-(0)7071-29 5059; E-mail: tilman.gocht@uni-tuebingen.de.

■ ACKNOWLEDGMENT

We thank Adam P. Hitchcock and Tom Regier for helpful discussion of our experiments, Sam Kalirai for measuring high-resolution gas-phase EELS-spectra, Chithra Karunakaran, Jian Wang and Yingshen Lu for providing excellent support at the CLS spectromicroscopy beamline 10ID-1. The STXM measurements described in this paper were performed at the Canadian Light Source, which is supported by the Natural Sciences and Engineering Research Council of Canada, the National Research Council Canada, the Canadian Institutes of Health Research, the Province of Saskatchewan, Western Economic Diversification Canada, and the University of Saskatchewan. The manuscript benefited from a critical review by Rainer Lohmann and three anonymous reviewers. This work was supported by the European Union FP6 Integrated Project AquaTerra (Project No. GOCE 505428), and the Norwegian Research Council KMB Project ACTIVE 192936 (Norwegian Geotechnical Institute).

■ REFERENCES

(1) Cornelissen, G.; Gustafsson, O.; Bucheli, T. D.; Jonker, M. T. O.; Koelmans, A. A.; Van Noort, P. C. M. Extensive sorption of organic compounds to black carbon, coal, and kerogen in sediments and soils: Mechanisms and consequences for distribution, bioaccumulation, and biodegradation. *Environ. Sci. Technol.* **2005**, *39* (18), 6881–6895.

(2) Lohmann, R.; MacFarlane, J. K.; Gschwend, P. M. Importance of black carbon to sorption of native PAHs, PCBs, and PCDDs in Boston and New York, Harbor sediments. *Environ. Sci. Technol.* **2005**, *39* (1), 141–148.

(3) Ahn, S.; Werner, D.; Luthy, R. G. Physicochemical characterization of coke-plant soil for the assessment of polycyclic aromatic hydrocarbon availability and the feasibility of phytoremediation. *Environ. Toxicol. Chem.* **2005**, *24* (9), 2185–2195.

(4) Oen, A. M. R.; Breedveld, G. D.; Kalaitzidis, S.; Christanis, K.; Cornelissen, G. How quality and quantity of organic matter affect polycyclic aromatic hydrocarbon desorption from Norwegian harbor sediments. *Environ. Toxicol. Chem.* **2006**, *25* (5), 1258–1267.

(5) Zimmerman, J. R.; Ghosh, U.; Millward, R. N.; Bridges, T. S.; Luthy, R. G. Addition of carbon sorbents to reduce PCB and PAH bioavailability in marine sediments: Physicochemical tests. *Environ. Sci. Technol.* **2004**, *38*, 5458–5464.

(6) Allen-King, R. M.; Grathwohl, P.; Ball, W. P. New modeling paradigms for the sorption of hydrophobic organic chemicals to heterogeneous carbonaceous matter in soils, sediments, and rocks. *Adv. Water Resour.* **2002**, *25* (8−12), 985–1016.

(7) Kwon, S.; Pignatello, J. J. Effect of natural organic substances on the surface and adsorptive properties of environmental black carbon (char): Pseudo pore blockage by model lipid components and its implications for N-2-probed surface properties of natural sorbents. *Environ. Sci. Technol.* **2005**, *39* (20), 7932–7939.

(8) Sander, M.; Pignatello, J. J. Characterization of charcoal adsorption sites for aromatic compounds: Insights drawn from single-solute and Bi-solute competitive experiments. *Environ. Sci. Technol.* **2005**, *39* (6), 1606–1615.

(9) Zhu, D. Q.; Pignatello, J. J. Characterization of aromatic compound sorptive interactions with black carbon (charcoal) assisted by graphite as a model. *Environ. Sci. Technol.* **2005**, *39* (7), 2033–2041.

(10) Ghosh, U.; Gillette, J. S.; Luthy, R. G.; Zare, R. N. Microscale location, characterization, and association of polycyclic aromatic hydrocarbons on harbor sediment particles. *Environ. Sci. Technol.* **2000**, *34* (9), 1729–1736.

(11) Gillette, J. S.; Luthy, R. G.; Clemett, S. J.; Zare, R. N. Direct observation of polycyclic aromatic hydrocarbons on geosorbents at the subparticle scale. *Environ. Sci. Technol.* **1999**, *33* (8), 1185–1192.

(12) Kalberer, M.; Morrical, B. D.; Sax, M.; Zenobi, R. Picogram quantitation of polycyclic aromatic hydrocarbons adsorbed on aerosol particles by two-step laser mass spectrometry. *Anal. Chem.* **2002**, *74* (14), 3492–3497.

(13) Zimmermann, R.; Ferge, T.; Galli, M.; Karlsson, R. Application of single-particle laser desorption/ionization time-of-flight mass spectrometry for detection of polycyclic aromatic hydrocarbons from soot particles originating from an industrial combustion process. *Rapid Commun. Mass Spectrom.* **2003**, *17* (8), 851–859.

(14) Lehmann, J.; Liang, B. Q.; Solomon, D.; Lerotic, M.; Luizao, F.; Kinyangi, J.; Schafer, T.; Wirick, S.; Jacobsen, C. Near-edge X-ray absorption fine structure (NEXAFS) spectroscopy for mapping nano-scale distribution of organic carbon forms in soil: Application to black carbon particles. *Global Biogeochem. Cycle* **2005**, *19* (1), 12.

(15) Lehmann, J.; Solomon, D.; Kinyangi, J.; Dathe, L.; Wirick, S.; Jacobsen, C. Spatial complexity of soil organic matter forms at nanometre scales. *Nat. Geosci.* **2008**, *1* (4), 238–242.

(16) Liang, B.; Lehmann, J.; Solomon, D.; Sohi, S.; Thies, J. E.; Skjemstad, J. O.; Luizao, F. J.; Engelhard, M. H.; Neves, E. G.; Wirick, S. Stability of biomass-derived black carbon in soils. *Geochim. Cosmochim. Acta* **2008**, *72* (24), 6069–6078.

(17) Yoon, T. H.; Benzerara, K.; Ahn, S.; Luthy, R. G.; Tyliszczak, T.; Brown, G. E. Nanometer-scale chemical heterogeneities of black carbon materials and their impacts on PCB sorption properties: Soft X-ray spectromicroscopy study. *Environ. Sci. Technol.* **2006**, *40* (19), 5923–5929.

(18) Endo, S.; Grathwohl, P.; Haderlein, S. B.; Schmidt, T. C. Effects of Native Organic Material and Water on Sorption Reference Diesel Soot. *Environ. Sci. Technol.* **2009**, *43* (9), 3187–3193.

(19) Kleineidam, S.; Schüth, C.; Grathwohl, P. Solubility-normalized combined adsorption-partitioning sorption isotherms for organic pollutants. *Environ. Sci. Technol.* **2002**, *36* (21), 4689–4697.

(20) NIST, Certificate of Analysis, Standard Reference Material 2975. In 2000.

(21) Harner, T.; Bidleman, T. F. Measurement of octanol-air partition coefficients for polycyclic aromatic hydrocarbons and polychlorinated naphthalenes. *J. Chem. Eng. Data* **1998**, *43* (1), 40–46.

(22) Jacobsen, C.; Wirick, S.; Flynn, G.; Zimba, C. Soft X-ray spectroscopy from image sequences with sub-100 nm spatial resolution. *J. Microsc.-Oxf* **2000**, *197*, 173–184.

(23) Hitchcock, A. P. *aXis2000; software available free for non-commercial use from* http://unicorn.mcmaster.ca/aXis2000.html.

(24) Hanhan, S.; Smith, A. M.; Obst, M.; Hitchcock, A. P. Optimization of analysis of soft X-ray spectromicroscopy at the Ca 2p edge. *J. Electron Spectrosc. Relat. Phenom.* **2009**, *173*, 44–49.

(25) Henke, B. L.; Gullikson, E. M.; Davis, J. C. X-ray interactions - photoabsorption, scattering, transmission, and reflection at $E = 50-30\,000$ eV, $Z = 1-92$. *Atom. Data Nucl. Data Tables* **1993**, *54* (2), 181–342.

(26) Molina, L.; Knoth, K.; Engel, S.; Holzapfel, B.; Eibl, O. Chemically deposited La2Zr2O7 buffer layers for YBCO-coated conductors: film growth and microstructure. *Supercond. Sci. Technol.* **2006**, *19* (11), 1200–1208.

(27) Zhu, X. L.; Eibl, O.; Scheideler, L.; Geis-Gerstorfer, J. Characterization of nano hydroxyapatite/collagen surfaces and cellular behaviors. *J. Biomed. Mater. Res., Part A* **2006**, *79A* (1), 114–127.

(28) Eyidi, D.; Croitoru, M. D.; Eibl, O.; Nemetschek, R.; Prusseit, W. Growth of CeO2 thin films deposited on biaxially textured nickel substrates. *J. Mater. Res.* **2003**, *18* (1), 14–26.

(29) Braun, A.; Mun, B. S.; Huggins, F. E.; Huffman, G. P. Carbon speciation of diesel exhaust and urban particulate matter NIST standard reference materials with C(1s) NEXAFS spectroscopy. *Environ. Sci. Technol.* **2007**, *41*, 173–178.

(30) Agren, H.; Vahtras, O.; Carravetta, V. Near-edge core photoabsorption in polyacenes—model molecules for graphite. *Chem. Phys.* **1995**, *196* (1−2), 47–58.

(31) Rouquerol, J.; Avnir, D.; Fairbridge, C. W.; Everett, D. H.; Haynes, J. H.; Pernicone, N.; Ramsay, J. D. F.; Sing, K. S. W.; Unger, K. K. Recommendations for the characterization of porous solids. *Pure Appl. Chem.* **1994**, *66* (8), 1739–1758.

(32) Dynes, J. J.; Tyliszczak, T.; Araki, T.; Lawrence, J. R.; Swerhone, G. D. W.; Leppard, G. G.; Hitchcock, A. P. Speciation and quantitative mapping of metal species in microbial biofilms using scanning transmission X-ray microscopy. *Environ. Sci. Technol.* **2006**, *40* (5), 1556–1565.

(33) Simonsen, J. B.; Handke, B.; Li, Z. S.; Moller, P. J. A study of the interaction between perylene and the TiO2(110)-(1 × 1) surface-based on XPS, UPS and NEXAFS measurements. *Surf. Sci.* **2009**, *603* (9), 1270–1275.

(34) Taborski, J.; Vaterlein, P.; Dietz, H.; Zimmermann, U.; Umbach, E. NEXAFS investigations on ordered adsorbate layers of large aromatic molecules. *J. Electron Spectrosc. Relat. Phenom.* **1995**, *75*, 129–147.

(35) Pignatello, J. J.; Kwon, S.; Lu, Y. F. Effect of natural organic substances on the surface and adsorptive properties of environmental black carbon (char): Attenuation of surface activity by humic and fulvic acids. *Environ. Sci. Technol.* **2006**, *40* (24), 7757–7763.